TABLE II
PARAMETERS OF THE ANALOG AND DIGITAL CHANNEL MODEL.[1] THE NUMERICAL VALUES OF ϵ_g AND ϵ_b REFER TO DPSK MODULATION WITH $E_{link}/N_0 = 10$ dB

Satellite Elevation	Environment	Antenna	A	10 log c	μ	σ	D_g	D_b	ϵ_g	ϵ_b
13°	Highway	C3	0.24	10.2 dB	−8.9 dB	5.1 dB	90 m	29 m	$1.6 \cdot 10^{-3}$	0.23
	City	C3	0.89	3.9 dB	−11.5 dB	2.0 dB	9 m	70 m	$1.4 \cdot 10^{-2}$	0.29
18°	City	C3	0.80	6.4 dB	−11.8 dB	4.0 dB	8 m	32 m	$7.2 \cdot 10^{-3}$	0.29
	City	D5	0.80	5.5 dB	−10.0 dB	3.7 dB	8 m	33 m	$9.5 \cdot 10^{-3}$	0.25
21°	New City	D5	0.57	10.6 dB	−12.3 dB	5.0 dB	45 m	60 m	$1.3 \cdot 10^{-3}$	0.30
	Highway	D5	0.03	16.6 dB	−7.1 dB	5.5 dB	524 m	15 m	$1.1 \cdot 10^{-4}$	0.19
	Highway	S6	0.03	18.1 dB	−7.9 dB	4.8 dB	514 m	17 m	$7.6 \cdot 10^{-5}$	0.20
24°	Old City	C3	0.66	6.0 dB	−10.8 dB	2.8 dB	27 m	52 m	$8.3 \cdot 10^{-3}$	0.27
	Old City	D5	0.78	9.3 dB	−12.2 dB	4.4 dB	21 m	76 m	$2.3 \cdot 10^{-3}$	0.30
	Old City	S6	0.79	11.9 dB	−12.9 dB	5.0 dB	24 m	88 m	$7.0 \cdot 10^{-4}$	0.32
	Highway	C3	0.25	11.9 dB	−7.7 dB	6.0 dB	188 m	62 m	$6.8 \cdot 10^{-4}$	0.20
	Highway	S6	0.19	17.4 dB	−8.1 dB	4.2 dB	700 m	160 m	$9.0 \cdot 10^{-5}$	0.21
34°	City	C3	0.58	6.0 dB	−10.6 dB	2.6 dB	24 m	33 m	$8.3 \cdot 10^{-3}$	0.27
	City	M2	0.72	10.0 dB	−11.9 dB	4.9 dB	21 m	55 m	$1.7 \cdot 10^{-3}$	0.29
	City	S6	0.60	9.5 dB	−12.2 dB	2.0 dB	20 m	31 m	$2.1 \cdot 10^{-3}$	0.31
	Highway	C3	0.008	11.7 dB	−8.8 dB	3.8 dB	1500 m	12 m	$7.6 \cdot 10^{-4}$	0.22
	Highway	S6	0.007	16.7 dB	−13.4 dB	5.3 dB	1500 m	11 m	$1.1 \cdot 10^{-4}$	0.32
43°	City	C3	0.54	5.5 dB	−13.6 dB	3.8 dB	42 m	49 m	$9.5 \cdot 10^{-3}$	0.34
	City	M2	0.65	11.0 dB	−15.4 dB	5.4 dB	16 m	29 m	$1.1 \cdot 10^{-3}$	0.36
	City	S6	0.56	6.5 dB	−15.6 dB	3.8 dB	51 m	65 m	$7.0 \cdot 10^{-3}$	0.38
	Highway	C3	0.002	14.8 dB	−12.0 dB	2.9 dB	8300 m	17 m	$2.0 \cdot 10^{-4}$	0.30
	Highway	M2	0.002	17.3 dB	−13.8 dB	2.0 dB	8300 m	17 m	$9.2 \cdot 10^{-4}$	0.35

[1]With respect to results listed in [15], this table contains some differences which are due to improved techniques of statistical evaluation.

density according to (5) and the corresponding distribution function are included in Figs. 4 and 5 as full lines. The fits show good agreement with the statistics of the recorded signal power. In Fig. 4 the Rician density which forms a pronounced peak at the power level of the unfaded satellite link can clearly be distinguished from the Rayleigh/log-normal density which increases for low power level. The distribution functions shown in Fig. 5 exhibit a bend at −1 dB for highway and at 4 dB for city, respectively. Above these levels the Rician fading (unshadowed areas) is predominant, characterized by the straight part of the line. At levels below the bend lognormal shadowing is present.

It may be expected that a transmission during shadowed intervals will not be successful with a realistic link budget. Therefore, the most important parameter of the land mobile satellite channel is the time-share of shadowing, A. $1\text{-}A$ is the time-share during which a transmission is possible and therefore represents a rough estimate for the achievable gross throughput of digital transmission systems. Fig. 8 shows the parameter $1\text{-}A$ for different satellite elevations. The symbols represent single recording experiments. The lines show that the time-share of unshadowed intervals, $1\text{-}A$ tends to increase with elevation (shadowing decreases). The values of $1\text{-}A$ indicate that on highways substantial data throughput can be achieved for all elevations tested, whereas in cities the throughput is rather small for low elevation.

During the periods without shadowing, the channel is modeled as a Rician channel (2), with the fading behavior described by Rice-factor c. Large values of c indicate few multipath fading ($c \to \infty$ for the Gaussian channel) resulting in good transmission characteristics. Small values of c correspond to severe fading ($c = 0$ for the Rayleigh channel).

B. Bit Error Rate for Continuous Transmission

The error probability of a received symbol is determined by the ratio of symbol energy E_s and one-sided noise power spectral density N_0. The received symbol energy E_s depends on the signal-to-noise ratio E_{link}/N_0 of the unfaded link and on the amount of shadowing and fading within the symbol duration. For reasonably high bit rates and realistic mobile speed v the fading varies slowly compared to the bit rate [18], then, the received signal power may be considered constant during one symbol interval. For a DPSK symbol received with momentary power S normalized to the power of the unfaded satellite link the error probability is

$$\mathrm{BER}(S) = \frac{1}{2} \exp\left(-SE_{link}/N_0\right). \tag{7}$$

With the probability density function $p(S)$ of the received power the mean BER becomes

$$\mathrm{BER} = \int_0^\infty \mathrm{BER}(S)\, p(S)\, dS. \tag{8}$$

The mean BER may be evaluated by numerical integration of (8), [15]. Based on (5), analytic expressions for the mean BER of DPSK and noncoherent FSK transmission are derived in [19].

Fig. 9 shows the resulting mean BER for DPSK transmission. The curves show that in shadowed areas, a prohibitively high link power would be necessary to reduce the BER to an acceptable range. In unshadowed areas a BER of 10^{-4} is achievable with moderate link power in spite of the presence of multipath fading. Using forward error correction (FEC) coding and interleaving, the link behavior may be improved

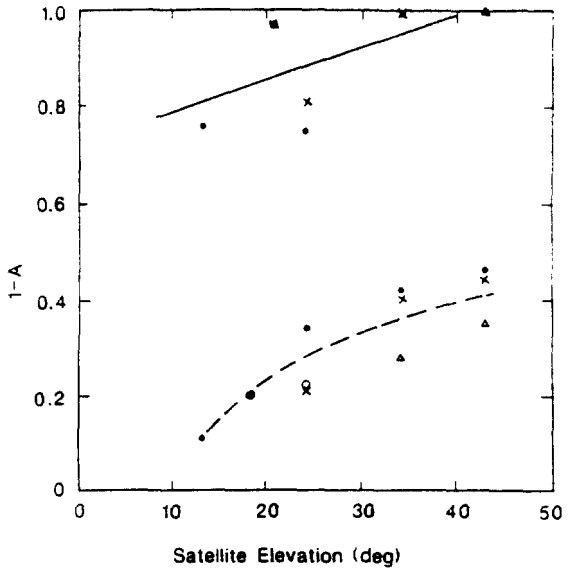

Fig. 8. Time-share of unshadowed time intervals versus satellite elevation. Lines represent all antennas.
- ● antenna C3
- △ antenna M2
- ○ antenna D5
- × antenna S6
- —— highway
- - - city.

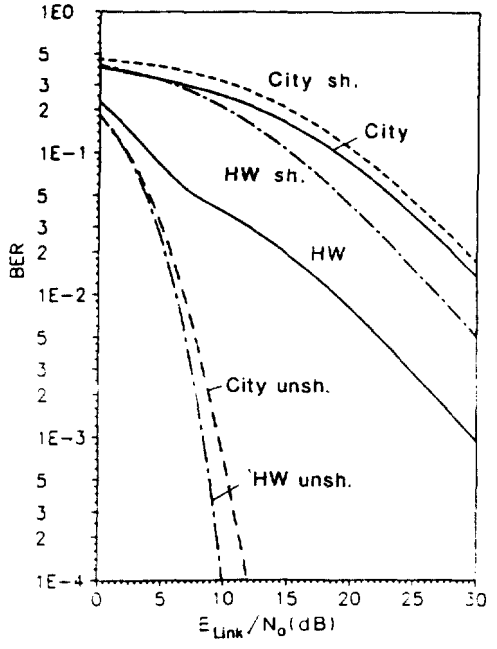

Fig. 9. Mean BER for DPSK transmission. Lines are showing BER for shadowed (sh.) and unshadowed (unsh.) areas in cities and on highways (HW). Full lines show combined BER. Antenna S6, 24° satellite elevation.

further [20]. The full lines in Fig. 9 show the BER averaged over both, shadowed and unshadowed areas.

C. Analog Model of the Land Mobile Satellite Channel

Fig. 10 shows a dynamic model of the land mobile satellite channel that reproduces the probability density function of the received signal power as well as the dynamic behavior of the fading and shadowing process. The transmitted signal $s(t)$ is deteriorated by multiplicative fading $a(t)$ and additive

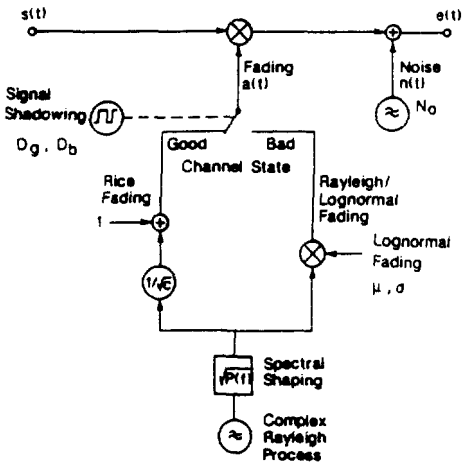

Fig. 10. Dynamic model of the land mobile satellite channel. The signals $s(t)$, $n(t)$, $e(t)$, and the fading process $a(t)$ are complex valued.

white Gaussian noise $n(t)$ with power spectral density N_0. The resulting received signal is

$$e(t) = s(t) \cdot a(t) + n(t). \tag{9}$$

It should be noted that the fading process $a(t)$ produced by the channel model is complex valued. The concept of multiplicative fading can be applied when the bandwidth of the transmitted signal is small compared to the coherence bandwidth of the fading. Measurements in urban environments [21] have shown that the coherence bandwidth of the land mobile channel is usually in the order of 100 kHz or larger. Therefore, the channel model according to Fig. 10 may be used for signal bandwidths up to several tens of kilohertz. Cochannel interference and adjacent channel interference are not considered in this paper, but may be easily included in the model if required.

According to Fig. 2 and Section III-A, the fading process $a(t)$ is "switched" between Rician fading, representing unshadowed areas with high received signal power (good channel state) and Rayleigh/lognormal fading, representing shadowed areas with low received signal power (bad channel state). This is a reasonable approximation to reality resulting in a simplified channel model. The characteristics of the switching process between shadowed and unshadowed sections can be approximated by a Markov model [22]. For a given speed v m/s and bit rate R b/s, the transition probabilities p_{gb} and p_{bg} can be related to the bit duration. According to the Markov model, the mean duration of a period of good (bad) channel state is given by

$$D_g \text{ bits} = \frac{1}{p_{gb}} = \frac{R}{v} D_g \text{ m}$$

$$D_b \text{ bits} = \frac{1}{p_{bg}} = \frac{R}{v} D_b \text{ m}. \tag{10}$$

The probability that a good (bad) channel state lasts longer than n bits is

$$p_g(>n) = p_{gg}^n$$

$$p_b(>n) = p_{bb}^n. \tag{11}$$

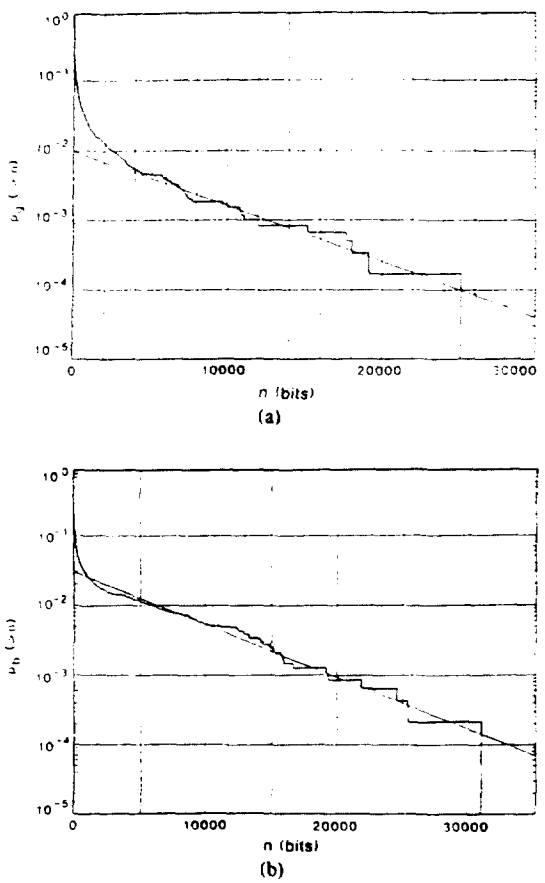

Fig. 11. Probability of the short-term mean received power staying above (a) or below (b) a threshold for more than n bit durations. The threshold corresponds to the time-share of shadowing, A. The probabilities are normalized such that $p_g(>0) = 1 - A$ and $p_b(>0) = A$. City environment, satellite elevation 21°, v = 40 km/h, R = 1200 b/s.

Plotting these probabilities in a semilogarithmic scale results in straight lines with slopes $\log p_{gg}$ and $\log p_{bb}$, respectively.

To verify if the shadowing process of the recorded channels can be approximated by a Markov model, the probability of the short-term mean received signal power staying above (below) a threshold for longer than n bit durations has been evaluated. Periods of the received signal power above and below the threshold are considered good and bad channel states, respectively. The threshold must be determined such that the time-share when the received signal power is below the threshold is equal to A. The time-share A of shadowing is known from curve fitting, Table II. The threshold can be determined from the probability distribution function of the received signal power. Fig. 11(a) and (b) shows probabilities of good (bad) channel states lasting longer than n bit in duration as evaluated from the recorded channel. The straight lines represent the approximation according to (11).

For short duration, the statistics of the recorded channel deviated from the straight lines. This is caused by level crossings due to fading. For longer duration, however, the Markov process is a good approximation. The transition probabilities of the Markov model can be derived from the probability distributions $p_g(>n)$ and $p_b(>n)$ of the recording by approximating them with straight lines, as shown in Figs. 11(a) and 11(b). The mean duration of a good (bad) channel state follows from (10), and

$$p_{gb} = 1 - p_{gg}$$
$$p_{bg} = 1 - p_{bb}. \tag{12}$$

The time-share of shadowing, A, is related to the durations D_g and D_b by

$$A = \frac{D_b}{D_g + D_b}. \tag{13}$$

The duration D_g and D_b evaluated from the distributions $p_g(>n)$ and $p_b(>n)$ usually do not satisfy (13) exactly. Therefore, mean values are computed according to

$$\overline{D_g} = \frac{1}{2}\left[D_g + \frac{1-A}{A}D_b\right]$$
$$\overline{D_b} = \frac{1}{2}\left[\frac{A}{1-A}D_g + D_b\right]. \tag{14}$$

For the measurements listed in Table II, the durations D_g m and D_b m were determined by (14).

Having described the dynamic behavior of the shadowing process, the fading process is considered below. As explained in Section III-A and indicated by Fig. 10, the received multipath signal may be modeled as a Rayleigh process having Rayleigh distributed amplitude and uniformly distributed phase. This process may be generated by complex addition of two independent stationary Gaussian processes. The spectral properties of the complex Rayleigh process are defined by an appropriate filter. In order to model the fading in city environments, a filter may be chosen that approximates [18, eq. (20)]. For rural environment, the filter should have a slowly decreasing low-pass characteristic as shown in Fig. 3(b). As a compromise, a flat low-pass filter with a bandwidth of maximum Doppler frequency may be used for all types of environments.

Based on the filtered Rayleigh process, the Rician fading is produced by attenuating the Rayleigh process to power of $1/c$ and adding a value of unity to represent the direct satellite signal component. The Rayleigh/lognormal fading is generated by multiplying the Rayleigh process with a slow lognormal shadowing process. This approach has the advantage that very deep fades can be reproduced which is not possible when assuming constant multipath power. Situations with partly shadowed line-of-sight signal are also included in the Rayleigh/log-normal fading. In order to approximate the dynamic behavior of the log-normal shadowing, the short-term mean received signal power S_0 may be chosen according to its probability density (4) independently for each shadowing interval and kept constant during that interval.

D. Digital Model of the Land Mobile Satellite Channel

Digital channel models describe the bit error process on the physical link and therefore give a higher level of abstraction. Due to the dominance of the shadowing process, the two-state Gilbert-Elliott model [23] appears very suitable for the land mobile satellite channel. The dynamics of the state

transitions are very similar to those described above for the transitions between the good and bad states in the analog model. Measurements and simulations have shown that the underlying Markov-chain can be described by the same probabilities p_{gb} and p_{bg} from (12) or by a state diagram in [24].

Once p_{gb} and p_{bg} are given, the bit error rate values ϵ_g and ϵ_b in the good and bad states, respectively, can be obtained [19]. The results are given in Table II for a DPSK signal with $E_{link}/N_0 = 10$ dB. The values of ϵ_g and ϵ_b may also be obtained from the stored channel measurements.

IV. Block Error Statistics and Model Comparison

In packet data communications, the blocks of data can be protected against transmission errors either by forward error correction (FEC) or by automatic repeat request (ARQ). For a plain ARQ scheme with error detection, the probability of a data block containing no errors is directly related to the throughput of the ARQ scheme. If a t-error correcting block code is applied, the probability of correct block decoding equals the probability of at most t errors occurring in the data block. Investigations concerning the achievable throughput of ARQ schemes as well as the optimization of code rate, signaling rate, and data block length are contained in [15] and [25]. No bit interleaving is assumed here because the bit error rate in the good state is reasonably low and in the bad state is very high. Without interleaving, it is possible to have a complete data block in an interval of good channel state. Thus an ARQ scheme exploits time intervals with good link characteristics for reliable data transmission.

Transmission channels with memory such as the land mobile satellite channel which has a strong statistical dependency among error gaps can be characterized by multigap distribution or by error correlation function [24], [26]. With error gap ν being the number of consecutive correctly received symbols between errors plus 1, the gap density $f_A(\nu)$ is defined as

$$f_A(\nu) = P(e_1 = 0 \cap e_2 = 0 \cap \cdots \cap e_{\nu-1} = 0 \cap e_\nu = 1 \mid e_0 = 1) \quad (15)$$

where e_i is 0 for an error-free symbol and 1 for an error.

The complementary gap distribution function $F_A(\nu)$ which is the probability of an error gap being larger than ν, is given by

$$F_A(\nu) = 1 - \sum_{j=1}^{\nu} f_A(j). \quad (16)$$

The gap density $f_A(j)$ is related to the block error density $P(m, n)$ by [26]

$$f_A(j) = \frac{1}{p}\left[P(0, j-1) - 2P(0, j) + P(0, j+1)\right], \quad (17)$$

where p is the mean bit error probability.

Inserting (17) into (16) and assuming that $P(0, 0) = 1$ and $P(0, 1) = 1 - p$, the complementary gap distribution function becomes

$$F_A(\nu) = \frac{P(0, \nu) - P(0, \nu + 1)}{p}. \quad (18)$$

The behavior of the recorded channel and its comparison with the channel models in terms of block error density $P(m, n)$, complementary gap distribution $F_A(\nu)$, and conditional block error probability $P_{F|F}$ will be given where $P_{F|F}$ is the probability that a block contains errors after decoding under the condition that the preceding block also contained errors. These criteria are well related to the transmission of data packets and are easy to measure in a real system. The error correlation function was not used because the calculation requirement was extensive, and the results did not show clearly the channel behavior in various environments.

For the digital model, the block error probability density $P(m, n)$ can be analytically derived from the state transition probabilities. With Z being the state "good" or "bad" and P_Z the state probability, $P(m, n)$ becomes

$$P(m, n) = \sum_{(Z)} P(m, n \mid Z) P_Z. \quad (19)$$

The conditional probabilities $P(m, n \mid Z)$ are calculated using recursion, starting with the first bit of a block. This result is found in [22] and [23] and is not repeated here. The block error probability density for the recorded measurements is directly determined by a window of blocklength n sliding along the measurement sequence and calculating the probability of m errors within the window. The average of all window results gives a very good approximation of the probability $P(m, n)$ as the number of samples is very large.

For two typical environments, city and highway, $P(m, n)$ is depicted in Fig. 12. Each diagram compares the results of the stored measurements, the analog model and the digital model for a block length of $n = 100$ bits. For small error numbers m, the models match the measurement curves very well. This region is of most interest because these few errors could be corrected by an error correcting code. The Gilbert–Elliott model exhibits a deep floor for the probability of 2–15 errors. The steep slope of the curve above its maximum stems from the fact that error events within the bad state are generated independently and that corresponds to the binomial distribution function. A comparison of the full line (recording) and the dashed line (simulation using the analog channel model) shows rather good agreement. This shows that the channel model, Fig. 10, not only reproduces the probability density function of the received signal power but models the dynamic behavior of the bit error sequence as well.

The information of the complementary gap distribution $F_A(\nu)$ is completely contained in the block error probability densities $P(m, n)$, $n = \nu, \nu + 1$ as indicated by (18). Fig. 13 shows $F_A(\nu)$ for the same recordings and channel models as Fig. 12. Here, the bad channel state corresponds to small values of ν, and the good channel state corresponds to large ν.

The performance of forward error correction is determined by the block error probability, P_F, that is, a block contains

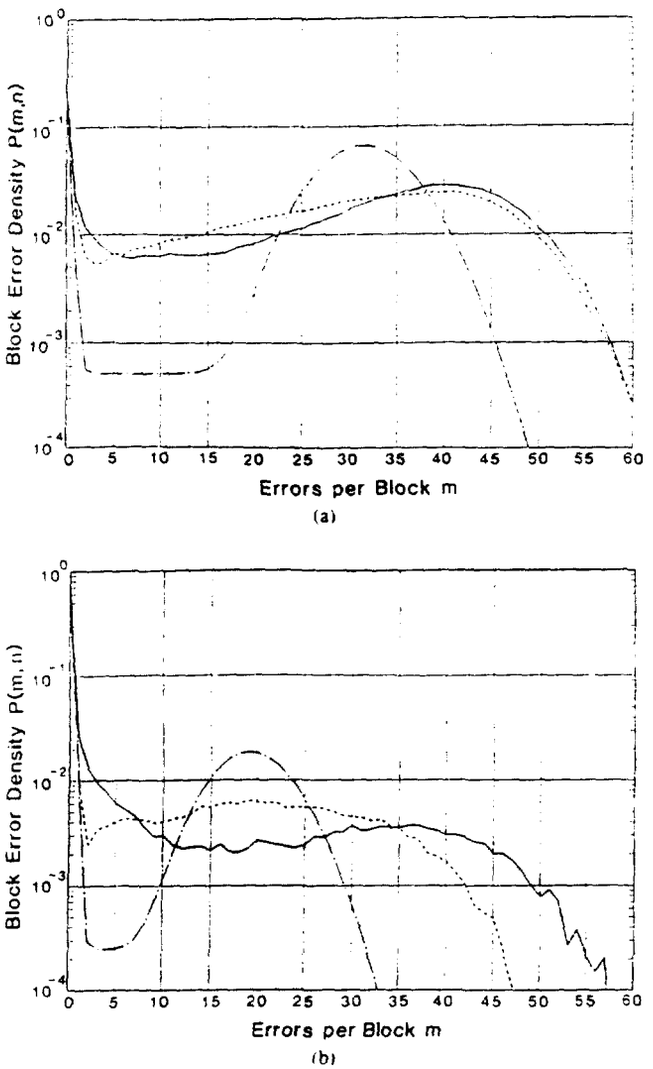

Fig. 12. Block error density $P(m, n)$. Satellite elevation 24°, blocklength $n = 100$ bits. $E_{link}/N_0 = 10$ dB, $R = 1200$ b/s. (a) City, antenna S6, $v = 40$ km/h. (b) Highway, antenna S6, $v = 90$ km/h.
—— channel recordings
- - - - analog channel model
····· Gilbert-Elliott model.

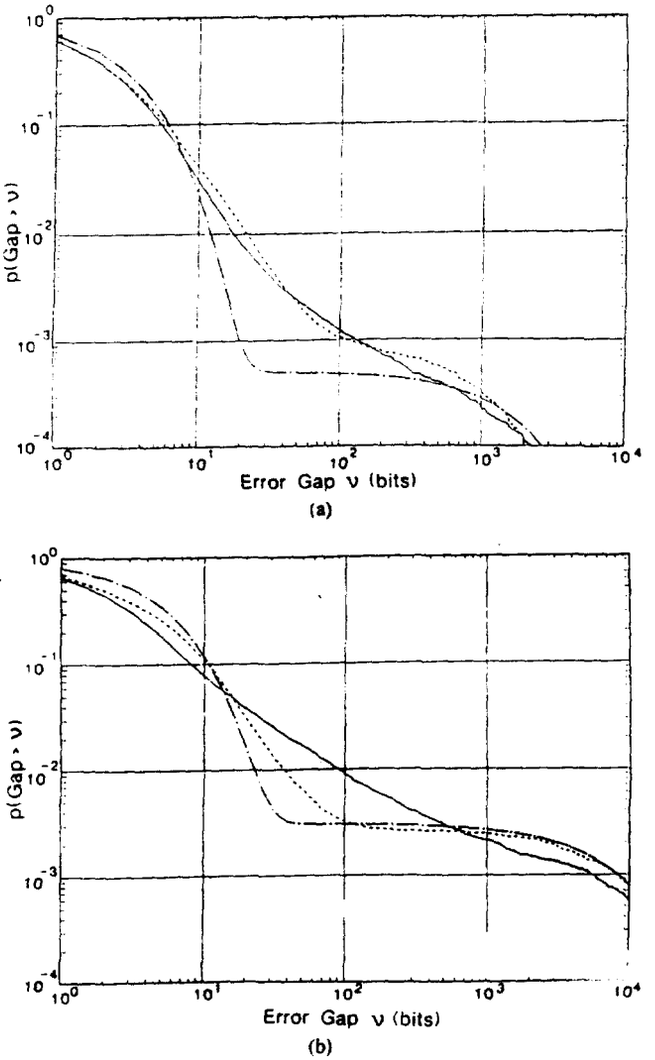

Fig. 13. Complementary error gap distribution $F_A(v)$. Satellite elevation 24°, $E_{link}/N_0 = 10$ dB, $R = 1200$ b/s. (a) City, antenna S6, $v = 40$ km/h. (b) Highway, antenna S6, $v = 90$ km/h.
—— channel recordings
- - - - analog channel model
····· Gilbert-Elliott model.

more errors than the code can correct. With bounded distance decoding, a block code can correct up to t errors in a block of length n and the block error probability, P_F can be calculated from

$$P_F = \sum_{m=t+1}^{n} P(m, n). \tag{20}$$

Due to very strong channel memory, a mean state duration is in the order of thousands of bits, and it is obvious that packet errors in succeeding blocks are highly dependent. This must be considered for the design of ARQ schemes. The dependence of block errors is shown by means of the conditional block error probability, $P_{F|F}$. For the Gilbert-Elliott model, $P_{F|F}$ can be analytically derived [22].

The curves of $P_{F|F}$ are shown in Fig. 14. The abscissa shows the distance between two defective blocks in bits. The conditional error curves, $P_{F|F}$ approach asymptotically the unconditioned block error probability, P_F which is 0.78 for city environment and 0.18 for highway. But, this happens only after the transmission of several thousands of bits. Long correlation is seen in the highway environment where $P_{F|F}$ is still greater than P_F after ten-thousand bits or an 8.3-s delay. In all cases, the models approximate reality quite well.

V. Conclusion

The land mobile satellite channel has been recorded and subjected to a statistical evaluation. An analog channel model was developed that can readily be used for fading simulation purposes. This channel model is largely characterized by the time-share of shadowing, A, and the Rice-factor, c, describing the channel during unshadowed periods. Alternatively, the land mobile satellite channel can be represented by a two-state Gilbert-Elliott model. A comparison of block error

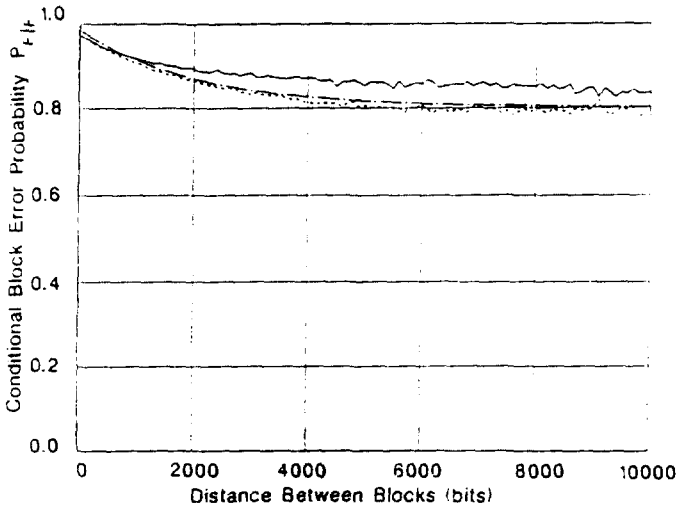

(a)

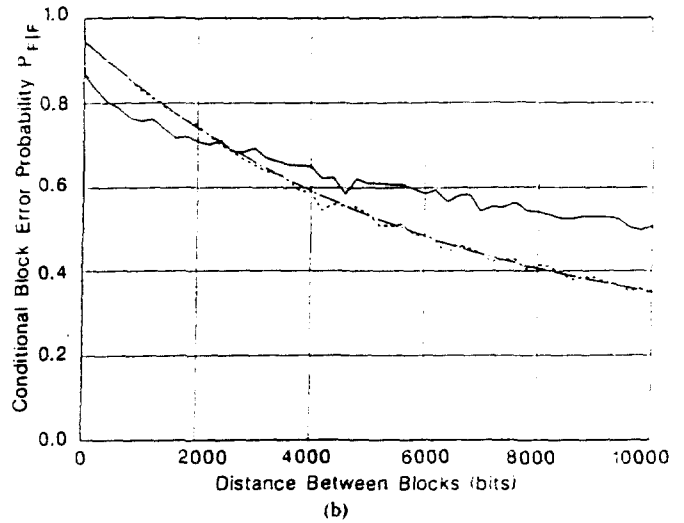

(b)

Fig. 14. Conditional block error probability $P_{F|F}$ versus block distance. Satellite elevation 24°, blocklength n = 100 b, t = 0, E_{link}/N_0 = 10 dB, R = 1200 b/s. (a) City, antenna S6, v = 40 km/h. (b) Highway, antenna S6, v = 90 km/h.
—— channel recordings
---- analog channel model
-·-·- Gilbert-Elliott model.

statistics shows good agreement between the recorded channel and the models. In combination with their parameter values, the developed channel models represent useful tools for the design and analysis of data transmission schemes. Moreover, the models show that reliable and efficient data transmission via the land mobile satellite channel should be achievable, if the transmission scheme is suitably adapted to the channel behavior.

Acknowledgment

The permission by ESA and INMARSAT to use the MARECS test carrier is acknowledged. The provision of antennas by the DLR institute of RF-techniques is appreciated. Furthermore, the authors would like to thank Prof. J. Hagenauer for valuable discussions and support.

References

[1] F. Naderi, "An advanced generation land mobile satellite system and its critical technologies," in *Proc. Nat. Telesystems Conf.*, TX, Nov. 1982.
[2] R. R. Lovell, G. H. Knouse, and W. J. Weber, "An experiment to enable commercial mobile satellite service," in *Proc. Nat. Telesystems Conf.*, TX, Nov. 1982.
[3] P. M. Bourdeau, R. W. Breithaupt, and J. L. McNally, "The Canadian mobile satellite program," in *Proc. Nat. Telesystems Conf.*, TX, Nov. 1982.
[4] S. Miura, "Experimental mobile satellite system for communications using Engineering Test Satellite-V (ETS-V/EMSS-C)," presented at the IAF '84, Lausanne, Switzerland, Oct. 1984.
[5] M. Wagg, "MOBILESAT, Australia's own," in *Proc. Int. Mobile Sat. Conf.*, Ottawa, Canada, June 1990.
[6] R. Rogard, "A land-mobile satellite system for digital communications in Europe," in *Proc. ESA Workshop*, Noordwijk, the Netherlands, June 1986.
[7] G. Berzins, "Communications on the move-INMARSAT's services in the future" in *Proc. Fourth Int. Conf. on Satellite Systems for Mobile Commun. and Navigation*, London, U.K., Oct. 1988.
[8] I. E. Casewell, I. C. Ferebee, and M. Tomlinsons, "A satellite paging system for land mobile users," in *Proc. Fourth Int. Conf. on Satellite Systems for Mobile Commun. and Navigation*, London, U.K., Oct. 1988.
[9] J. Hagenauer and E. Lutz, "Forward error correction coding for fading compensation in mobile satellite channels," *IEEE J. Select. Areas Commun.*, vol. SAC-5, pp. 215-225, Feb. 1987.
[10] G. C. Hess, "Land-mobile satellite excess path loss measurements," *IEEE Trans. Veh. Technol.*, vol. VT-29, pp. 290-297, May 1980.
[11] C. Loo, "Measurements and models of a land mobile satellite channel and their applications to MSK signals," *IEEE Trans. Veh. Technol.*, vol. VT-35, pp. 114-121, Aug. 1987.
[12] J. S. Butterworth, "Propagation measurements for land mobile satellite systems at 1542 MHz," CRC Tech. Note 723, Ottawa, Canada, Aug. 1984.
[13] W. C. Y. Lee, *Mobile Communications Design Fundamentals*. Indianapolis, IN: Howard W. Sams, 1986.
[14] J. Hagenauer and W. Papke, "Data transmission for maritime and land mobiles using stored channel simulation," in *Proc. IEEE 32nd Veh. Technol. Conf. 1982*, San Diego, CA, pp. 379-383.
[15] E. Lutz, W. Papke, and E. Plöchinger, "Land mobile satellite communications—channel model, modulation and error control," in *Proc. 7th Int. Conf. on Digital Satellite Commun. 1986*, Munich, Germany, pp. 537-543.
[16] F. Hansen and F. Meno, "Mobile fading—Rayleigh and lognormal superimposed," *IEEE Trans. Veh. Technol.*, vol. VT-26, pp. 332-335, Nov. 1977.
[17] C. Loo, "A statistical model for a land mobile satellite link," *IEEE Trans. Veh. Technol.*, vol. VT-34, pp. 122-127, Aug. 1985.
[18] R. H. Clarke, "A statistical theory of mobile radio reception," *Bell Syst. Tech. J.*, vol. 47, pp. 957-1000, July/Aug. 1968.
[19] D. Cygan, "Analytical evaluation of average bit error rate for the land mobile satellite channel," *Int. J. Satell. Commun.*, vol. 7, pp. 99-102, Apr. 1989.
[20] E. Lutz, "Code and interleaver design for data transmission over fading channels," in *Proc. GLOBECOM '84*, Atlanta, GA, pp. 381-386.
[21] D. C. Cox and R. P. Leck "Correlation bandwidth and delay spread multipath propagation statistics for 910 MHz urban mobile radio channels," *IEEE Trans. Commun.*, vol. COM-23, pp. 1271-1280, Nov. 1975.
[22] D. Cygan, M. Dippold, and J. Finkenzeller, "Models for the land mobile satellite channel," *Archiv. Elec. Übertr.*, vol. 42, pp. 329-339, Nov. Dec. 1988.
[23] E. O. Elliott, "Estimates of error rates for codes on burst-noise channels," *Bell Syst. Tech. J.*, vol. 42, pp. 1977-1997, Sept. 1963.
[24] L. N. Kanal and A. R. K. Sastry, "Models for channels with memory and their applications to error control," *Proc. IEEE*, vol. 66, pp. 724-744, July 1978.
[25] E. Lutz, "Simulation of FEC/ARQ data transmission using stored land mobile satellite channels," in *Proc. IEEE 36th Veh. Technol. Conf. 1986*, Dallas, TX, pp. 109-115.
[26] J.-P.A. Adoul, "Error intervals and cluster density in channel modeling," *IEEE Trans. Inform. Theory*, vol. IT-20, pp. 125-129, Jan. 1974.